Hindawi
Geofluids
Volume 2021, Article ID 6621643, 10 pages
https://doi.org/10.1155/2021/6621643

Research Article

Estimating Macrofracture Toughness of Sandstone Based on Nanoindentation

Zilong Zhou, Boxiang Lei, Xin Cai, and Yichao Rui

School of Resources and Safety Engineering, Central South University, Changsha 410083, China

Correspondence should be addressed to Xin Cai; xincai@csu.edu.cn

Received 24 December 2020; Revised 8 January 2021; Accepted 15 January 2021; Published 27 January 2021

Academic Editor: Bin Gong

Copyright © 2021 Zilong Zhou et al. This is an open access article distributed under the Creative Commons Attribution License, which permits unrestricted use, distribution, and reproduction in any medium, provided the original work is properly cited.

An upscaling method for estimating macrofracture toughness by nanoindentation results was proposed in this study. Grid nanoindentation tests were conducted on sandstone samples to obtain micromechanical properties of indents, including elastic modulus, hardness, and stiffness. Multifactor cluster analysis was then carried out to categorize the sandstone into five mechanical phases. Finally, the macrofracture toughness was predicted by using the macroelastic modulus of the sample and the critical energy release rate of the weakest phase. To verify this method, the upscaling result was compared with the macrofracture toughness measured by the notched semicircular bending (NSCB) test. The discrepancy in the macrofracture toughness from our method and the NSCB test was 8.8%, which was acceptable. Also, it is proved that our method can provide more accurate upscaling results compared to other methods.

1. Introduction

As known to all, the macromechanical properties of rock materials are very important for the design and construction of rock engineering, such as macroelastic modulus and macrofracture toughness [1–4]. The former is commonly obtained from unconfined compressive tests [5–7] and the latter from specific fracture tests, such as the short rod test [8] and notched semicircular bending (NSCB) test [9–13]. However, under some particular circumstances, it is very hard or high cost to manufacture the rock samples meeting the testing requirements (such as size and shape) [14]. As an economical, nondestructive, and repeatable testing method, the nanoindentation technique only requires a small amount of material without specific requirements in sample size and shape to measure microscopic parameters [15, 16], such as microelastic modulus, hardness, and fracture toughness. Based on this, the macroparameters of rock can be estimated. Therefore, how to exactly upgrade microscopic parameters into macroscopic ones is of great significance to practical applications.

To date, a great effort has been made towards macroscopic parameters upscaling from nanoindentation data [15, 17–25]. For example, Li et al. [24] determined the microelastic moduli of different phases in concrete by nanoindentation. They further used the Mori-Tanaka (MT) scheme to estimate the macroelastic modulus of concrete. Gao et al. [25] found that the microelastic modulus of each phase is crucial for homogenization estimation. A slight variation in the microelastic modulus of a phase can significantly change the macroelastic modulus of material. Kong et al. [15] compared the macroelastic modulus of 3D printed rocks upgraded by the MT scheme, Self-Consistent Scheme (SCS) method, and Differential Effective Medium (DEM) method. They reported that the upscaling results from the MT scheme and SCS method are closer to the macroelastic modulus obtained from the unconfined compressive test. Liu et al. [26] estimated the macroelastic modulus by combining the grid nanoindentation and deconvolution with the Mori-Tanaka scheme. The discrepancy between the values from the unconfined compression test and upgrading method was less than 15%.

The above mentioned research studies concentrated on the estimation of macroelastic modulus. Fracture toughness, reflecting the resistance for crack initiation and propagation [27, 28], is another crucial parameter for rock fragmentation

and hydrofracturing [29–32]. At the microscopic level, the fracture toughness of indents can be determined by the crack length method [33] or energy method [26, 34–36] based on nanoindentation results. It is documented that the microfracture toughness of indents holds a linear relation with its microelastic modulus. However, limited studies can be found in predicting macrofracture toughness from microscopic parameters. To et al. [37] regarded the microfracture toughness of the weakest phase as the macrofracture toughness of glass-ceramic nanocomposite. They found that the estimated value agrees with the value obtained from the macrofracture test. Liu et al. [34] predicted the macrofracture toughness of the Bakken shale by the average value of microfracture toughness of all indents. In the two studies, the microfracture toughness of indents is directly used to estimate the macrofracture toughness of material without any theoretical foundation. The results estimated by these methods are suspicious. Therefore, the upscaling method for the macrofracture toughness of inhomogeneous materials (e.g., rock-like materials) should be further improved.

In this research, we proposed an upscaling method for macrofracture toughness of rock material from nanoindentation results based on the Griffith fracture criterion. Firstly, the micromechanical parameters of each indent including elastic modulus, hardness, and stiffness were calculated after grid nanoindentation tests; secondly, the multifactor cluster analysis was conducted to distinguish mechanical phases according to the similarity of micromechanical parameters of indents; thirdly, assuming that the crack proceeds from the weakest mechanical phase, the macrofracture toughness was estimated based on the homogenized elastic modulus of rock samples and the critical energy release rate of the weakest phase; finally, the upscaling result was compared with the macrofracture toughness measured by the notched semicircular bending (NSCB) test to verify the effectiveness of this method.

2. Methods

2.1. Proposed Upscaling Method

2.1.1. Upscaling Method for Macrofracture Toughness Based on the Griffith Theory. According to the Griffith fracture criterion [38], the critical fracture energy release rate for an open crack (G) is

$$G = \frac{K^2}{E}, \tag{1}$$

where K is the fracture toughness and E is the elastic modulus. Hence, the macrofracture toughness of rock (K_{IC}^{ma}) can be expressed as

$$K_{IC}^{ma} = \sqrt{G_{ma} E_{ma}}, \tag{2}$$

where G_{ma} and E_{ma} are the macrocritical energy release rate and elastic modulus of the rock sample, respectively.

As a typical nonhomogeneous material, rock is composed of different mechanical phases. It is assumed that the fracture primarily proceeds from the weakest phase in the rock sample so that the critical energy release rate of the sample (G_{ma}) can be approximated by that of the weakest phase (G_{min}). Thus, the macrofracture toughness of rock samples can be estimated by

$$K_{IC}^{ma} = \sqrt{G_{min} E_{ma}}. \tag{3}$$

The value of G_{min} was calculated as the average value of the microcritical energy release rate of all indents in the weakest phase. The mechanical phases in the rock sample are distinguished by multifactor cluster analysis, which is introduced in the next section.

For multiphase inclusion mixtures, the elastic modulus of the sample (E_{ma}) can be calculated as [21]

$$E_{ma} = \frac{9K_{hom}G_{hom}}{3K_{hom} + G_{hom}}, \tag{4}$$

where K_{hom} and G_{hom} are the homogenization bulk modulus and homogenization shear modulus, respectively. They can be expressed by [21]

$$\begin{cases} K_{hom} = \dfrac{\sum_{i=1}^{n} f_i \bullet K_i (1 + \alpha_0 ((K_i/K_0) - 1))^{-1}}{\sum_{i=1}^{n} f_i \bullet (1 + \alpha_0 \bullet ((K_i/K_0) - 1))^{-1}}, \\ G_{hom} = \dfrac{\sum_{J=1}^{n} f_i \bullet G_i (1 + \beta_0 ((G_i/G_0) - 1))^{-1}}{\sum_{J=1}^{n} f_i \bullet (1 + \beta_0 \bullet ((G_i/G_0) - 1))^{-1}}, \end{cases} \tag{5}$$

where K_0 and G_0 are the bulk modulus and shear modulus of the reference medium; in this paper, quartz was selected as the reference medium; thus, $K_0 = 41.1$ GPa and $G_0 = 37.4$ GPa [39]; $\alpha_0 = 3K_0/(3K_0 + 4G_0)$ and $\beta_0 = (6K_0 + 12G_0)/(15K_0 + 20G_0)$; K_i and G_i are the bulk modulus and shear modulus of the i-th phase; f_i is the volume fraction of the i-th phase. K_i and G_i can be calculated by

$$\begin{cases} G_i = \dfrac{E^i}{2(1+\nu)}, \\ K_i = \dfrac{E^i}{3(1-\nu)}, \end{cases} \tag{6}$$

where E^i is the microelastic modulus of the i-th phase; ν is the Poisson ratio of phases, $\nu = 0.25$ in this research.

2.1.2. Classification of Mechanical Phases in Rock. As an important method in data mining, the clustering technique can partition a dataset into a meaningful set of mutually exclusive clusters according to the similarity of data to make the data more similar within groups and more diverse between groups [40]. In this study, clustering analysis was conducted to distinguish the mechanical phases within the rock sample based on the K-means algorithm [41] and further obtain the value of G_{min} in Equation (3). For more accurate results, three microparameters of each indent, including elastic modulus (E), hardness (H), and stiffness (S) measured

in nanoindentation tests, were selected as the classification parameters.

The K-means algorithm includes the following steps: (1) determine the clustering number n through the elbow method [42, 43]; (2) select n initial clustering centers stochastically and partition the objects to the nearest clustering center to form a cluster according to the nearest-neighbor rule; (3) compute the mean value of each cluster (i.e., the new clustering center) [41]; (4) repeat procedures (2) and (3) in SPSS software until the sum of squared errors (SSE) is minimum; then, we can determine the clustering center under the clustering number n. The SSE is determined as

$$\mathrm{SSE} = \sum_{i=1}^{n} \sum_{p \in C_i} (p - m_i)^2, \tag{7}$$

where p is the object in space; m_i is the center of cluster C_i. The smaller the SSE, the higher the similarity within group data.

2.2. Experimental Setup and Procedure

2.2.1. Rock Material Characterization. In this study, a fine-grained sandstone collected from Kunming city (Yunnan province, China) is selected as test material. The mineral composition of the sandstone is determined by an Energy-Dispersive X-ray spectrometer (EDX MLA250) in our prior publication [44]. The sandstone has 42.74% quartz, 16.85% omphacite, 13.90% calcite, 11.19% hematite, 9.08% feldspar, and 4.89% clay. Several basic physical properties of the sandstone are measured as follows: density 2374 kg•m^{-3}, water absorption 3.5%, porosity 8.87%, and P-wave velocity 2812 m/s. Moreover, unconfined compressive tests were performed on cylindrical sandstone samples, which indicates that the sandstone holds the uniaxial compressive strength of 46.99 MPa and the elastic modulus of 7.21 GPa.

2.2.2. Nanoindentation Test

(1)Sample Preparation. Miller et al. [45] pointed out that the surface roughness of the sample greatly affects the accuracy of test data in nanoindentation tests; i.e., the smoother the sample surface, the smaller the measured data dispersion. Thus, the surface of rock samples should be polished elaborately. The procedure of sample preparation includes the following steps (see Figure 1):

(1) *Cutting*. Divide sandstone block into small pieces of 1-2 cm

(2) *Resin Inlay*. Put rock pieces in moulds and then pour the specific resin solution into the moulds. After curing for three hours, the rock pieces were stably half-embedded in the epoxy resin. Cylindrical samples with 3 cm in diameter and 2 cm in height were then taken out from the moulds

(3) *Mechanical Polishing*. The samples were elaborately ground by using a semiautomatic polishing machine (Struers Tegramin-25). Sand disks with different particle sizes were applied with a gradual transition from coarse to fine grinding to ensure the top and bottom ends of samples were parallel to each other

(2)Grid Test Based on Nanoindentation. Nanoindentation tests were conducted on a nanoindenter (Hysitron Triboindenter, Hysitron Inc., USA) with a load resolution of 3 nN and a displacement resolution of 0.04 nm at the School of Materials Science and Engineering in Xiangtan University. As shown in Figure 2, a matrix of 100 indents covering 450 $\times$ 450 μm^2 on the sample surface was chosen for tests. The distance between neighboring indents was set to be 50 μm to avoid the influence of neighboring indents [46].

Figure 3 illustrates the loading scheme in nanoindentation tests. The load increases to the maximum value of 350 mN, followed by a holding step with a duration of 15 s. The holding step is necessary for accurate experimental results [35]. After that, the load gradually decreases to zero. The loading and unloading rates are constant at 35 mN/s.

(3)Calculation of Micromechanical Parameters and Microfracture Toughness. Figure 4(a) shows a standard P-h curve of an indent in the nanoindentation test. From which, some basic micromechanical parameters can be further obtained, such as microelastic modulus (E_{mi}), stiffness (S), and hardness (H), residual indentation depth (h_{f}), maximum indentation depth (h_{m}), and indentation depth of beginning holding step (h_{l}) [47].

The indentation hardness (H) and reduced elastic modulus (E_{r}) can be calculated as

$$\begin{cases} H = \dfrac{P_{\max}}{A}, \\ E_{\mathrm{r}} = \dfrac{\sqrt{\pi} S}{2\beta\sqrt{A}}, \end{cases} \tag{8}$$

where $P_{\max}$ is the maximum value of the load, A is the contact area, and β is the geometric constant of the Berkovich indenter ($\beta = 1.034$). If the effects of nonrigidity on the measurements of elastic modulus are neglected, the microelastic modulus (E_{mi}) of indents can be represented by the reduced elastic modulus [36]. Otherwise, it should be calculated by [47]

$$\frac{1 - \nu^2}{E_{\mathrm{mi}}} = \frac{1}{E_{\mathrm{r}}} - \frac{1 - \nu_{\mathrm{in}}{}^2}{E_{\mathrm{in}}}, \tag{9}$$

where ν and E_{r} are the Poisson ratio and reduced elastic modulus of the sample, respectively; ν_{in} and E_{in} are the Poisson ratio and elastic modulus of the indenter, respectively. For the Berkovich indenter, $\nu_{\mathrm{in}} = 0.07$ and $E_{\mathrm{in}} = 1140$ GPa [26]. Also, for the tested sandstone, $\nu = 0.25$.

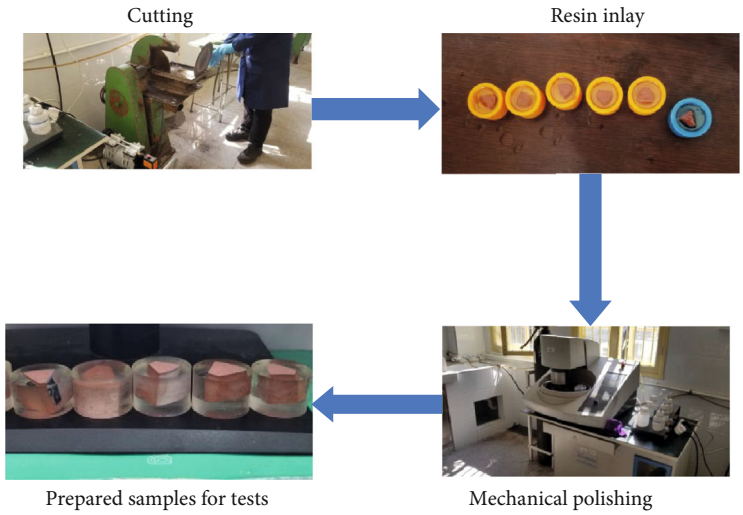

Figure 1: Sample preparation in the nanoindentation test.

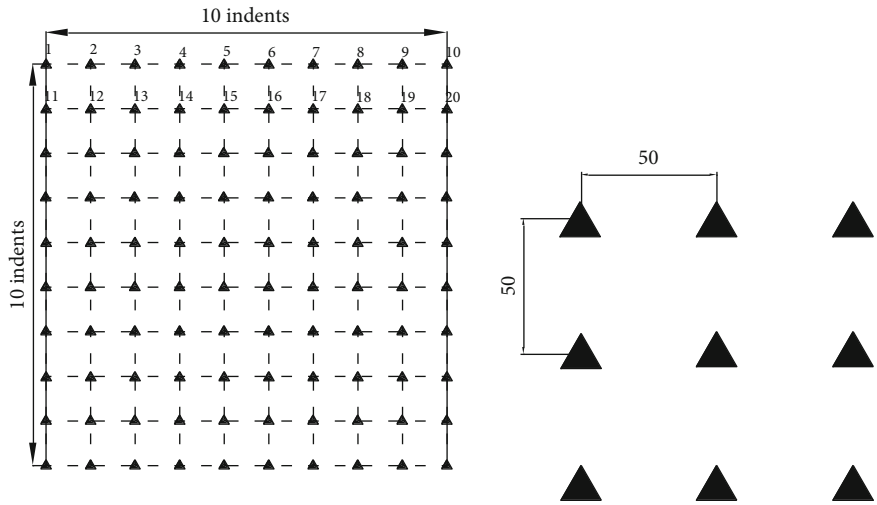

Figure 2: Schematic of the indent matrix.

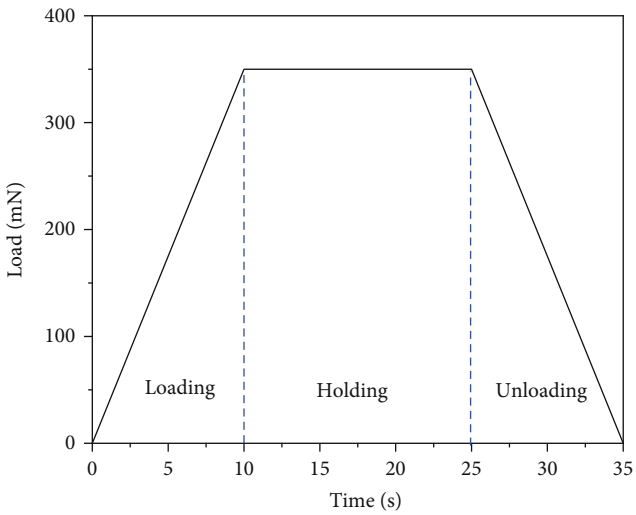

Figure 3: Schematic diagram of the loading scheme.

The microfracture toughness (K_{IC}^{mi}) of each indent is calculated by [26]

$$K_{IC}^{mi} = \sqrt{G_c E_r}, \tag{10}$$

where G_c is the critical energy release rate and E_r is the reduced elastic modulus. The G_c can be expressed by [26]

$$G_c = \frac{W_c}{A_{max}}, \tag{11}$$

where W_c is the fracture energy and A_{max} is the maximum crack area. For the Berkovich indenter, $A_{max} = 24.5h_m^2$. The constant load phase of the P-h curve is smooth without any fluctuation, which indicates that cracks do not develop significantly. Therefore, we can consider the contact area between the indent and the material as the maximum crack area. According to the energy conservation law, if tiny energy

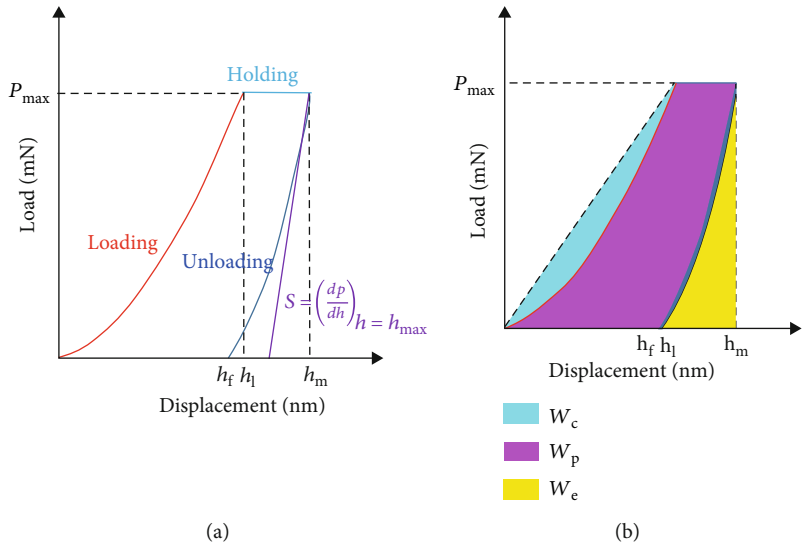

Figure 4: Schematic of the (a) standard *P-h* curve and (b) energy partition.

(such as heat and acoustic energy) is ignored, the W_c can be estimated as [26]

$$W_c = W_t - W_e - W_p, \tag{12}$$

where W_t, W_e, and W_p are the total energy, elastic energy, and plastic energy, as depicted in Figure 4(b). They can be calculated as [35, 48]

$$\begin{cases} W_t = \int_0^{h_l} P_{loading} dh + \int_{h_l}^{h_{max}} P_{holding} dh, \\ W_e = \int_{h_f}^{h_{max}} P_{unloading} dh, \\ W_p = \left[1 - \dfrac{(1+m)(1-h_f/h_m)}{(1+n)(1+m(1-h_l/h_m))}\right] W_t, \end{cases} \tag{13}$$

where n and m are fitting constants for the loading and unloading curves; $P_{loading}$ is the function of the loading curve; $P_{unloading}$ is the function of the unloading curve; $P_{holding}$ is the load during the holding stage, which is 350 mN in this research. The function of loading and unloading curves can be expressed as [47]

$$\begin{cases} P_{loading} = ah^m, \\ P_{unloading} = b(h - h_f)^n. \end{cases} \tag{14}$$

Substituting Equations (11)–(14) into Equation (10), the microfracture toughness of each indent in the sandstone sample can be obtained.

2.2.3. Macro-Quasi-Static Fracture Toughness Test. To validate our proposed method, we carried out notched semicircular bending (NSCB) tests to obtain the macrofracture toughness of the sandstone. The schematic view of the NSCB sample is shown in Figure 5. The loading speed is maintained at 0.05 mm/min. The actual macrofracture toughness of the sandstone (K_{IC}) can be calculated as [9]

$$K_{IC} = Y' \frac{P_m \sqrt{\pi l_n}}{2RB}, \tag{15}$$

where P_m is the maximum loads on the NSCB sample; l_n is the notch length; B and R are the thickness and radius of the sample, respectively; Y' is a nondimensional stress intensity factor related to sample geometry as [9]

$$\begin{aligned} Y' = &-1.297 + 9.516\alpha - (0.47 + 16.457\alpha)\beta \\ &+ (1.071 + 34.401\alpha)\beta^2, \end{aligned} \tag{16}$$

where $\alpha = S/2R$; $\beta = l_n/R$; S is the distance between the two supporting pins. A total of five NSCB tests were conducted. The average fracture toughness is 0.51 MPa·m$^{0.5}$.

3. Results and Discussion

3.1. Multifactor Cluster Results

3.1.1. Determination of the Optimal Clustering Number. Figure 6 presents the variation of the minimum SSE versus clustering number (n). It can be clearly seen that with the rise of the clustering number, the minimum SSE first decreases sharply and then decreases slowly. The elbow point occurs at $n = 5$. According to the elbow method, the optimal clustering number should be five. In other words, the nanoindentation results of the sandstone can be divided into five different mechanical phases. The 3D diagrams of the final clustering results are shown in Figure 7.

3.1.2. Clustering Center. In this study, the clustering center of each mechanical phase is determined by iteration using SPSS software. The initial clustering center is stochastically generated. After every iteration, the clustering center will be changed until the SSE value becomes stable. To characterize the

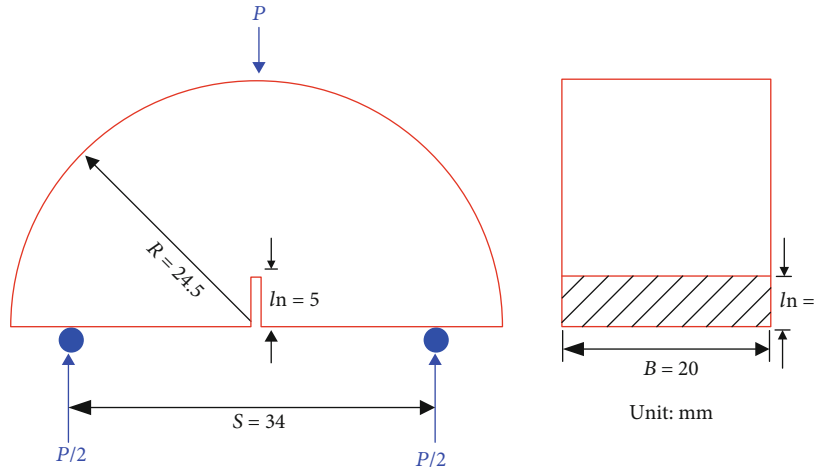

Figure 5: Schematic of the NSCB sample.

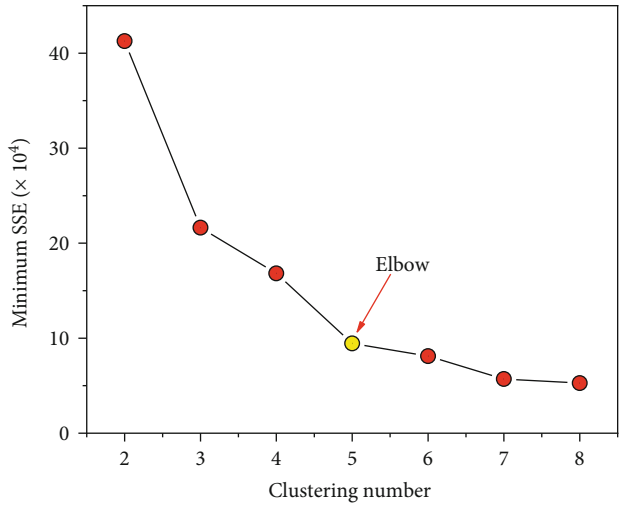

Figure 6: The relationship between the minimum SSE and the n value.

variation of the clustering center, the change distance of the clustering center after the n-th iteration (D_n) in the Cartesian coordinate system was introduced as

$$D_n = \sqrt{(E_{n+1} - E_n)^2 + (H_{n+1} - H_n)^2 + (S_{n+1} - S_n)^2}, \quad (17)$$

where E_n, H_n, and S_n are the elastic modulus, hardness, and stiffness of the clustering center in the n-th clustering iteration.

Figure 8 depicts the change distance of the clustering center versus the number of iterations. Evidently, except for phase 5, the change distances of the clustering center for the other four phases gradually decrease with the increasing number of iterations in six iterations. After that, the value of D_n is equal to zero. This means that the clustering center does not change anymore. As shown in Figure 7, the clustering center of phase 5 is 776.21 μN/nm in stiffness, 154.50 GPa in elastic modulus, and 17.66 GPa in hardness. The indentation response with the strongest phase in the sandstone likely presents hematite minerals. However, phase 1 with a clustering center of 397.35 μN/nm in stiffness, 23.00 GPa in elastic modulus, and 2.72 GPa in hardness is the weakest in the sandstone, which could be due to the presence of clay minerals. Therefore, the value of $G_{\min}$ in Equation (3) should be that of phase 1.

3.2. Upscaling Results of the Fracture Toughness of Sandstone

3.2.1. Microfracture Parameters of Each Mechanical Phase. In our study, for each mechanical phase, the microfracture toughness is calculated by the average energy release rate (G_a^i) (i.e., the average value of the energy release rate of all indents in the respective phase) and the elastic modulus of the i-th phase's clustering center (E^i) as

$$K_{IC}^i = \sqrt{G_a^i E^i}. \quad (18)$$

Figure 9 depicts the energy release rate and microfracture toughness of five phases. We can clearly observe that for the sandstone, the average energy release rate of the mechanical phase is between 0.032 and 0.353 mN·nm/nm^2, and the fracture toughness ranges from 0.85 to 7.25 MPa·m$^{0.5}$. Generally, the higher the average energy release rate, the greater the microfracture toughness. Except for phase 5, it holds the maximum fracture toughness but has the second energy release rate. This may be due to the fact that there is only one datum of indent categories into phase 5.

3.2.2. Comparison between Upscaling Results and NSCB Results. As discussed above, the critical energy release rate ($G_{\min}$) of the weakest phase (phase 1) should be 0.032 mN·nm/nm^2. According to Equations (4)–(6), the upscaling macroelastic modulus (E_{ma}) of the sandstone is 6.75 GPa, which fairly approximates the elastic modulus obtained from uniaxial compression tests (7.21 GPa). Substituting calculated values of $G_{\min}$ and E_{ma} into Equation (3), the upscaling fracture toughness of the sandstone is obtained as 0.465 MPa·m$^{0.5}$. The difference between the

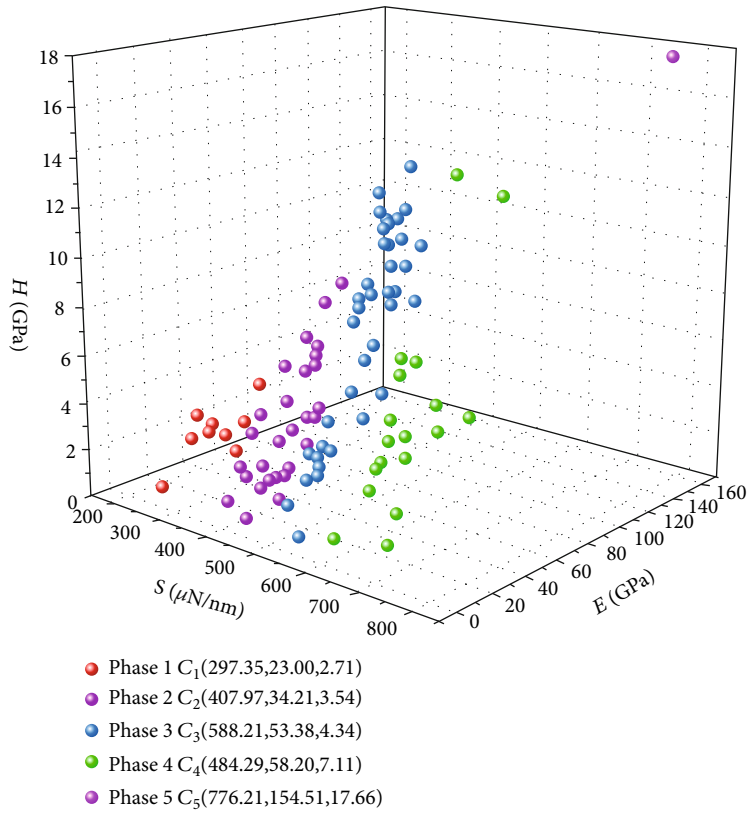

Figure 7: 3D diagram of the final clustering results of the sandstone (the colorful dots present different mechanical phases of the sandstone).

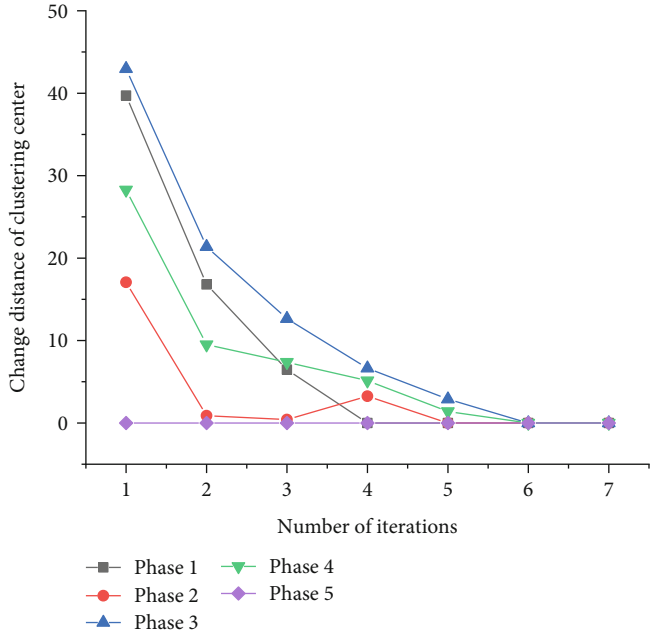

Figure 8: The relationship between the change distance of the clustering center and the number of iterations.

upscaling value and the NSCB tested value (0.51 MPa·m$^{0.5}$) is within an acceptable scale (10%). Therefore, it is proved that our proposed method is effective for fracture toughness upscaling. It can be also found that the upscaling fracture toughness is about 8.8% lower than that measured in NSCB tests. This may be due to the heterogeneity of the sandstone. In fact, on newly formed fracture surfaces, not only the weakest phase exists but also other phases do. This would result in the higher apparent fracture toughness obtained in NSCB tests.

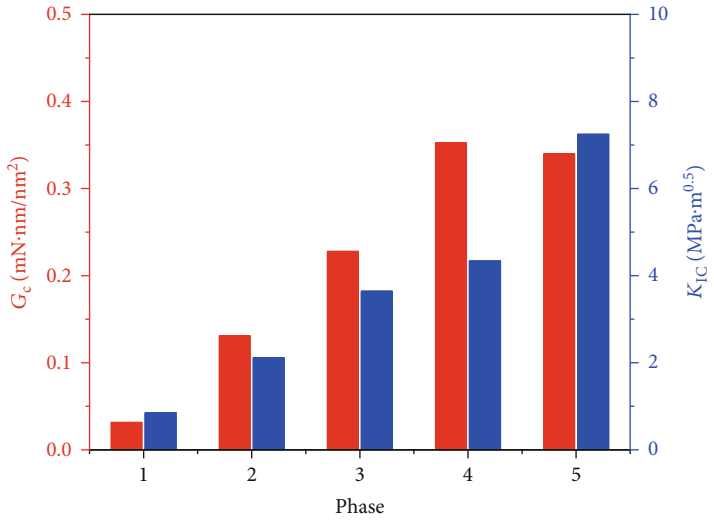

Figure 9: Microfracture energy release rate and fracture toughness of each phase.

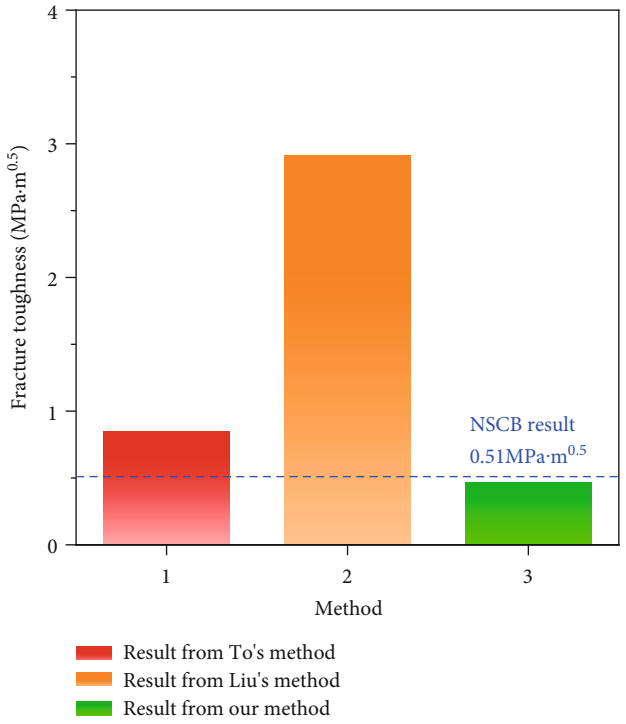

Figure 10: Upscaling results of fracture toughness by different methods.

Figure 10 shows the upscaling fracture toughness by three methods for comparison. In method 1 [37], the upscaling value is the minimum fracture toughness of the phase (0.85 MPa·m$^{0.5}$). This is 1.67 times greater than the NSCB tested value. Method 2 is proposed by Liu et al. [34]. They take the average fracture toughness of all tested indents as the macrofracture toughness. By this method, the upscaling fracture toughness is 2.91 MPa·m$^{0.5}$, even 5.71 times greater than the NSCB tested value. Among the three methods, the upscaling fracture toughness by our proposed method holds the least deviation with the real macrofracture toughness of the sandstone. Hence, our proposed method is suggested to be applied to estimate macrofracture toughness of rock materials from nanoindentation results.

4. Conclusions

In the present study, an upscaling method for macrofracture toughness based on nanoindentation tests is proposed. Firstly, nanoindentation tests are performed on sandstone samples to obtain micromechanical parameters of indents, including elastic modulus, hardness, and stiffness. Secondly, the three microparameters are used in multifactor cluster analysis to classify nanoindentation data into several mechanical phases. Thirdly, the macroelastic modulus of the sample is estimated by the Mori-Tanaka scheme, and the critical energy release rate is calculated by the average value of the energy release rate of all indents in the weakest phase. Finally, the macrofracture toughness is upgraded based on the energy method. Compared with the macrofracture toughness measured in NSCB tests and the upscaling results from other methods, it is proved that our proposed method can estimate the macrofracture toughness of rock more accurately.

Data Availability

The data can be provided if it is requested.

Conflicts of Interest

The authors declare that there is no conflict of interest regarding the publication of this paper.

Acknowledgments

This work was supported by the National Natural Science Foundation of China (41772313), the Hunan Science and Technology Planning Project (No. 2019RS3001), and the Fundamental Research Funds for Central Universities of the Central South University (2019zzts682).

References

[1] F. Song, A. Rodriguez-Dono, S. Olivella, and Z. Zhong, "Analysis and modelling of longitudinal deformation profiles of tunnels excavated in strain-softening time-dependent rock masses," *Computers and Geotechnics*, vol. 125, article 103643, 2020.

[2] B. Liu, Y. Song, K. Zhu, P. Su, X. Ye, and W. Zhao, "Mineralogy and element geochemistry of salinized lacustrine organic-rich shale in the Middle Permian Santanghu Basin: implications for paleoenvironment, provenance, tectonic setting and shale oil potential," *Marine and Petroleum Geology*, vol. 120, article 104569, 2020.

[3] D. Ma, J. Zhang, H. Duan et al., "Reutilization of gangue wastes in underground backfilling mining: overburden aquifer protection," *Chemosphere*, vol. 264, part 1, article 128400, 2021.

[4] X. Cai, Z. Zhou, H. Zang, and Z. Song, "Water saturation effects on dynamic behavior and microstructure damage of sandstone: phenomena and mechanisms," *Engineering Geology*, vol. 276, article 105760, 2020.

[5] Z. T. Bieniawski and M. J. Bernede, "Suggested methods for determining the uniaxial compressive strength and deformability of rock materials. Part 1. Suggested method for determination of the uniaxial compressive strength of rock materials," *International Journal of Rock Mechanics and Mining Sciences & Geomechanics Abstracts*, vol. 16, no. 2, pp. 138–140, 1979.

[6] K. Du, X. Li, M. Tao, and S. Wang, "Experimental study on acoustic emission (AE) characteristics and crack classification during rock fracture in several basic lab tests," *International Journal of Rock Mechanics and Mining Sciences*, vol. 133, article 104411, 2020.

[7] B. Gong, Y. Jiang, and L. Chen, "Feasibility investigation of the mechanical behavior of methane hydrate-bearing specimens using the multiple failure method," *Journal of Natural Gas Science and Engineering*, vol. 69, article 102915, 2019.

[8] M. D. Wei, F. Dai, N. W. Xu, Y. Liu, and T. Zhao, "A novel chevron notched short rod bend method for measuring the mode I fracture toughness of rocks," *Engineering Fracture Mechanics*, vol. 190, pp. 1–15, 2018.

[9] M. D. Kuruppu, Y. Obara, M. R. Ayatollahi, K. P. Chong, and T. Funatsu, "ISRM-suggested method for determining the mode I static fracture toughness using semi-circular bend specimen," *Rock Mechanics and Rock Engineering*, vol. 47, no. 1, pp. 267–274, 2014.

[10] M.-D. Wei, F. Dai, N.-W. Xu, Y. Liu, and T. Zhao, "Fracture prediction of rocks under mode I and mode II loading using the generalized maximum tangential strain criterion," *Engineering fracture mechanics*, vol. 186, pp. 21–38, 2017.

[11] X. Cai, Z. Zhou, L. Tan, H. Zang, and Z. Song, "Fracture behavior and damage mechanisms of sandstone subjected to wetting-drying cycles," *Engineering Fracture Mechanics*, vol. 234, article 107109, 2020.

[12] X. P. Zhou and Y. T. Wang, "Numerical simulation of crack propagation and coalescence in pre-cracked rock-like Brazilian disks using the non-ordinary state-based peridynamics," *International Journal of Rock Mechanics and Mining Sciences*, vol. 89, pp. 235–249, 2016.

[13] M. M. Kou, Y. J. Lian, and Y. T. Wang, "Numerical investigations on crack propagation and crack branching in brittle solids under dynamic loading using bond-particle model," *Engineering Fracture Mechanics*, vol. 212, pp. 41–56, 2019.

[14] B. Liu, Y. Yang, J. Li, Y. Chi, J. Li, and X. Fu, "Stress sensitivity of tight reservoirs and its effect on oil saturation: a case study of Lower Cretaceous tight clastic reservoirs in the Hailar Basin, Northeast China," *Journal of Petroleum Science and Engineering*, vol. 184, article 106484, 2020.

[15] L. Kong, M. Ostadhassan, S. Zamiran, B. Liu, C. Li, and G. G. Marino, "Geomechanical upscaling methods: comparison and verification via 3D printing," *Energies*, vol. 12, no. 3, 2019.

[16] Z. Zhou, X. Cai, X. Li, W. Cao, and X. Du, "Dynamic response and energy evolution of sandstone under coupled static–dynamic compression: insights from experimental study into deep rock engineering applications," *Rock Mechanics and Rock Engineering*, vol. 53, no. 3, pp. 1305–1331, 2020.

[17] C. Wang, Y. Wu, and J. Xiao, "Three-scale stochastic homogenization of elastic recycled aggregate concrete based on nano-indentation digital images," *Frontiers of Structural and Civil Engineering*, vol. 12, no. 4, pp. 461–473, 2018.

[18] W. R. L. Da Silva, J. Němeček, and P. Štemberk, "Methodology for nanoindentation-assisted prediction of macroscale elastic properties of high performance cementitious composites," *Cement and Concrete Composites*, vol. 45, pp. 57–68, 2014.

[19] W. R. L. Da Silva, J. Němeček, and P. Štemberk, "Application of multiscale elastic homogenization based on nanoindentation for high performance concrete," *Advances in Engineering Software*, vol. 62–63, pp. 109–118, 2013.

[20] L. Brown, P. G. Allison, and F. Sanchez, "Use of nanoindentation phase characterization and homogenization to estimate the elastic modulus of heterogeneously decalcified cement pastes," *Materials & Design*, vol. 142, pp. 308–318, 2018.

[21] K. Liu, M. Ostadhassan, B. Bubach, K. Ling, B. Tokhmechi, and D. Robert, "Statistical grid nanoindentation analysis to estimate macro-mechanical properties of the Bakken Shale," *Journal of Natural Gas Science and Engineering*, vol. 53, pp. 181–190, 2018.

[22] V. Kumar, M. E. Curtis, N. Gupta, C. H. Sondergeld, and C. S. Rai, "Estimation of Elastic Properties of Organic Matter and Woodford Shale Through Nano-indentation Measurements," in *SPE Canadian Unconventional Resources Conference*, Calgary, Alberta, Canada, October 2012.

[23] C. Li, M. Ostadhassan, L. Kong, and B. Bubach, "Multi-scale assessment of mechanical properties of organic-rich shales: a coupled nanoindentation, deconvolution analysis, and homogenization method," *Journal of Petroleum Science and Engineering*, vol. 174, pp. 80–91, 2019.

[24] Y. Li, Y. Li, and R. Wang, "Quantitative evaluation of elastic modulus of concrete with nanoidentation and homogenization method," *Construction and Building Materials*, vol. 212, pp. 295–303, 2019.

[25] X. Gao, Y. Wei, and W. Huang, "Effect of individual phases on multiscale modeling mechanical properties of hardened cement paste," *Construction and Building Materials*, vol. 153, pp. 25–35, 2017.

[26] K. Liu, M. Ostadhassan, and B. Bubach, "Applications of nano-indentation methods to estimate nanoscale mechanical properties of shale reservoir rocks," *Journal of Natural Gas Science and Engineering*, vol. 35, no. Part A, pp. 1310–1319, 2016.

[27] M. Kou, X. Liu, S. Tang, and Y. Wang, "3-D X-ray computed tomography on failure characteristics of rock-like materials under coupled hydro-mechanical loading," *Theoretical and Applied Fracture Mechanics*, vol. 104, article 102396, 2019.

[28] Y. T. Wang, X. P. Zhou, and M. M. Kou, "Three-dimensional numerical study on the failure characteristics of intermittent fissures under compressive-shear loads," *Acta Geotechnica*, vol. 14, no. 4, pp. 1161–1193, 2019.

[29] B. Gong, Y. Jiang, P. Yan, and S. Zhang, "Discrete element numerical simulation of mechanical properties of methane hydrate-bearing specimen considering deposit angles," *Journal of Natural Gas Science and Engineering*, vol. 76, article 103182, 2020.

[30] X. Cai, Z. Zhou, L. Tan, H. Zang, and Z. Song, "Water saturation effects on thermal infrared radiation features of rock materials during deformation and fracturing," *Rock Mechanics and Rock Engineering*, vol. 53, no. 11, pp. 4839–4856, 2020.

[31] S. Wang, X. Li, J. Yao et al., "Experimental investigation of rock breakage by a conical pick and its application to non-explosive mechanized mining in deep hard rock," *International Journal of Rock Mechanics and Mining Sciences*, vol. 122, article 104063, 2019.

[32] S. Wang, L. Sun, X. Li et al., "Experimental investigation of cuttability improvement for hard rock fragmentation using conical cutter," *International Journal of Geomechanics*, vol. 21, no. 2, article 06020039, 2021.

[33] D. Ma, L. Sun, T. Gao, J. Wang, and L. Wang, "New method for extracting fracture toughness of ceramic materials by instrumented indentation test with Berkovich indenter," *Journal of the European Ceramic Society*, vol. 37, no. 6, pp. 2537–2545, 2017.

[34] K. Liu, M. Ostadhassan, C. Li, A. Alexeyev, and X. Hou, "Fracture Toughness Measurement of Shales Using Nano-Indentation: The Bakken Case Study," in *The 51st U.S. Rock Mechanics/Geomechanics Symposium*, San Francisco, California, USA, June 2017.

[35] Q. Zeng, Y. Feng, and S. Xu, "A discussion of 'Application of nano-indentation methods to estimate nanoscale mechanical properties of shale reservoir rocks' by K Liu, M Osatadhassan and B Bubach," *Journal of Natural Gas Science and Engineering*, vol. 42, pp. 187–189, 2017.

[36] C. Sun, G. Li, M. E. Gomah, J. Xu, and H. Rong, "Meso-scale mechanical properties of mudstone investigated by nanoindentation," *Engineering Fracture Mechanics*, vol. 238, article 107245, 2020.

[37] T. To, C. Stabler, E. Ionescu, R. Riedel, F. Célarié, and T. Rouxel, "Elastic properties and fracture toughness of SiOC-based glass-ceramic nanocomposites," *Journal of the American Ceramic Society*, vol. 103, no. 1, pp. 491–499, 2019.

[38] C. T. Sun and Z.-H. Jin, *Chapter 2- Griffith Theory of Fracture*, C. T. Sun and Z.-H. B. T.-F. M. Jin, Eds., Academic Press, Boston, 2012.

[39] J. G. Berryman, "Elastic behavior of random polycrystals composed of anisotropic α-quartz (SiO_2) under pressure," *International Journal of Engineering Science*, vol. 89, pp. 121–132, 2015.

[40] Z. Zhang, J. Zhang, and H. Xue, "Improved K-means clustering algorithm," in *2008 Congress on Image and Signal Processing*, vol. 5, pp. 169–172, Sanya, Hainan, 2008.

[41] U. Maulik and S. Bandyopadhyay, "Genetic algorithm-based clustering technique," *Pattern recognition*, vol. 33, no. 9, pp. 1455–1465, 2000.

[42] A. Likas, N. Vlassis, and J. J. Verbeek, "The global k-means clustering algorithm," *Pattern recognition*, vol. 36, no. 2, pp. 451–461, 2003.

[43] R. Nainggolan, R. Perangin-Angin, E. Simarmata, and A. F. Tarigan, "Improved the performance of the K-means cluster using the sum of squared error (SSE) optimized by using the elbow method," *Journal of Physics: Conference Series*, vol. 1361, no. 1, 2019.

[44] Z. Zhou, X. Cai, D. Ma, W. Cao, L. Chen, and J. Zhou, "Effects of water content on fracture and mechanical behavior of sandstone with a low clay mineral content," *Engineering Fracture Mechanics*, vol. 193, pp. 47–65, 2018.

[45] M. Miller, C. Bobko, M. Vandamme, and F. J. Ulm, "Surface roughness criteria for cement paste nanoindentation," *Cement and Concrete Research*, vol. 38, no. 4, pp. 467–476, 2008.

[46] P. Sudharshan Phani and W. C. Oliver, "A critical assessment of the effect of indentation spacing on the measurement of hardness and modulus using instrumented indentation testing," *Materials & Design*, vol. 164, article 107563, 2019.

[47] W. C. Oliver and G. M. Pharr, "Measurement of hardness and elastic modulus by instrumented indentation: advances in understanding and refinements to methodology," *Journal of materials research*, vol. 19, no. 1, pp. 3–20, 2004.

[48] X. Su, P. Chen, and T. Ma, "Evaluation of shale fracture toughness based on micrometer indentation test," *Petroleum*, vol. 5, no. 1, pp. 52–57, 2019.